Correlation of Structural, Morphological, Magnetic, and CV Features in $CoFe_2O_4$ and $NiFe_2O_4$ Thin Films

Yuvraj R. Lingayat[1], Santosh D. More[2], Bhagwat A. Shelke[3], Chandrashekhar M. Kale[4]

[1,2]PG and Research Centre, Deogiri College, Chhatrapati Sambhajinagar
[3]Vivekanand Arts sardar Dalipsingh commerce and science college Chhatrapati Sambhajinagar,
[4]Indraraj Arts, Commerce and Science College, Sillod. Dist. Chhatrapati Sambhajinagar 431112(MS)-India

Abstract

This work compares the structural, morphological, magnetic and electrochemical behavior of $CoFe_2O_4$ and $NiFe_2O_4$ thin films prepared under identical spray pyrolysis conditions. X-ray diffraction confirms the formation of the spinel phase in both systems, with $CoFe_2O_4$ showing sharper and more intense reflections, indicating relatively higher crystallinity. AFM imaging reveals that $CoFe_2O_4$ develops a rougher surface, while $NiFe_2O_4$ exhibits a smoother topography with narrower height distributions. VSM measurements show that $CoFe_2O_4$ attains higher magnetization throughout the applied field range than $NiFe_2O_4$. Cyclic voltammograms recorded at different scan rates display increasing current response for both films, and $CoFe_2O_4$ consistently delivers higher current densities. These graphical trends demonstrate clear differences in microstructure, magnetic strength and redox activity between the two ferrite systems and highlight how the choice of divalent cation governs their functional performance.

Keywords: thin films, Spinel ferrites. Spray pyrolysis, Magnetic properties, Electrochemical behavior

Introduction

Spinel ferrites remain important for applications that rely on controlled magnetic and redox behavior [1–3]. Their stable crystal framework, mixed-valence states and tunable cation distribution make them suitable for electronic, magnetic and electrochemical devices [4,5]. Among these materials, $CoFe_2O_4$ and $NiFe_2O_4$ are widely examined because they combine structural stability with characteristic magnetic properties and electrochemical activity [6–8]. When developed as thin films, their performance depends strongly on crystallinity, surface texture and magnetic ordering [9].

X-ray diffraction (XRD) provides information on phase formation, preferred orientation and crystallite size, all of which influence magnetic interactions and charge transport [10]. Atomic force microscopy (AFM) helps assess surface quality, grain arrangement and roughness, which play a role in domain behavior and interfacial processes [11]. Magnetic measurements carried out using vibrating sample magnetometry (VSM) give insight into coercivity, magnetization and anisotropy, which depend on

microstructure and cation distribution [12]. Cyclic voltammetry (CV) supports the understanding of redox activity in ferrites through the Fe^{2+}/Fe^{3+} and Co^{2+}/Co^{3+} or Ni^{2+}/Ni^{3+} couples, offering a direct evaluation of their charge-storage capability [13,14].
A comparative examination of $CoFe_2O_4$ and $NiFe_2O_4$ thin films through these techniques provides a clear view of how structural and surface features influence magnetic and electrochemical behavior. This combined approach helps establish the structure property relationship needed for thin-film materials intended for magnetic components or redox-active electrodes [15].

2. Experimental details

2.1 Experimental procedure

Analytical-grade metal nitrates were used as precursors for both ferrite systems. For $NiFe_2O_4$, ferric nitrate nonahydrate [$Fe(NO_3)_3·9H_2O$] and nickel nitrate hexahydrate [$Ni(NO_3)_2·6H_2O$] were dissolved in double-distilled water in a 1:2 molar ratio (Ni:Fe). For $CoFe_2O_4$, cobalt nitrate hexahydrate [$Co(NO_3)_2·6H_2O$] and ferric nitrate nonahydrate were used in the same stoichiometric proportion. The precursor concentration for $NiFe_2O_4$ was varied from 0.03 M to 0.12 M, while $CoFe_2O_4$ was prepared using a fixed 0.1 M solution. Each salt was dissolved separately, combined, and stirred for 15 minutes before adding an equal volume of ethanol to enhance spray formation and droplet stability.
Glass and FTO substrates were ultrasonically cleaned prior to deposition. All films were deposited using a computer-controlled spray pyrolysis system operated at a constant substrate temperature of 450°C. The spray rate was maintained at 3–4 ml/min, the nozzle-to-substrate distance was fixed at 30 cm, and atmospheric air was used as the carrier gas. These parameters were kept identical for both ferrite systems to enable a direct comparison of their structural and functional characteristics.
The $NiFe_2O_4$ films prepared at different precursor molarities were labeled NF-C1, NF-C2, NF-C3, and NF-C4. The $CoFe_2O_4$ films deposited under the same conditions were labeled CF-1. All samples were subsequently analyzed using X-ray diffraction (XRD), atomic force microscopy (AFM), vibrating sample magnetometry (VSM), and cyclic voltammetry (CV).

3. Characterizations

The structural properties of the $CoFe_2O_4$ and $NiFe_2O_4$ thin films were examined using X-ray diffraction (XRD) with Cu–Kα radiation ($\lambda = 1.5406$ Å). The diffraction patterns were used to confirm the formation of the spinel phase and to estimate crystallite size and lattice parameters [16,17]. Surface topography and grain features were studied using atomic force microscopy (AFM) operated in tapping mode. AFM images helped evaluate grain distribution, roughness and the effect of film composition on the surface structure [18]. Magnetic measurements were carried out using a vibrating sample magnetometer (VSM) at room temperature. Hysteresis curves were recorded to determine saturation magnetization, coercivity and remanence, which reflect cation distribution and microstructural features of the ferrite films [19,20]. Electrochemical behaviour was evaluated using cyclic voltammetry (CV) in a three-electrode configuration. The ferrite thin film deposited on a conducting substrate was used as the working electrode, platinum served as the counter electrode and Ag/AgCl as the reference electrode. All measurements were performed in 1 M KOH electrolyte. CV curves recorded at different scan rates were used to assess redox activity and to calculate the specific capacitance of both $CoFe_2O_4$ and $NiFe_2O_4$ films [21].

3.1 X-ray diffraction analysis

The crystal structure of the spray-deposited $CoFe_2O_4$ and $NiFe_2O_4$ thin films was examined by X-ray diffraction, and the corresponding patterns are presented in Fig. 1. Both samples show the expected reflections of a single-phase cubic spinel structure, indexed to the (111), (220), (311), (400), (422), (511), (440), and (533) planes [16]. These peaks match well with standard JCPDS data for spinel ferrites, confirming that phase-pure $CoFe_2O_4$ and $NiFe_2O_4$ were obtained [17]. In both films, the (311) reflection is the most intense, which is typical for this class of materials [22].

The $CoFe_2O_4$ film exhibits sharper and more intense peaks than $NiFe_2O_4$, indicating higher crystallinity and better long-range ordering [23]. In contrast, the broader peaks in the $NiFe_2O_4$ pattern point to smaller crystallite size and greater lattice strain [24]. These differences likely arise from variations in cation distribution and the decomposition behavior of the respective metal precursors during spray pyrolysis. The calculated lattice parameters fall within the expected range for spinel ferrites, confirming the formation of the cubic phase [17].

Overall, the XRD results show that $CoFe_2O_4$ develops a more crystalline structure, while $NiFe_2O_4$ tends toward a nanocrystalline state. This structural contrast is consistent with the trends observed in AFM, VSM, and CV analyses discussed in later sections.

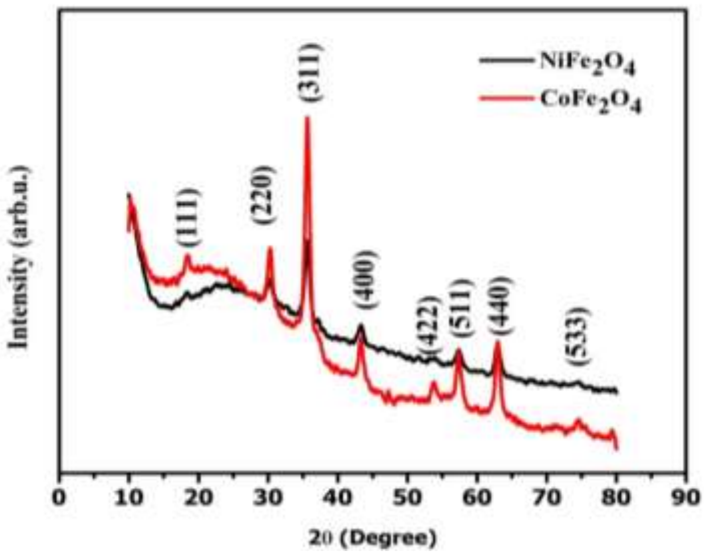

Fig.1. XRD patterns of NiFe2O4 and CoFe2O4 thin films.

3.2 AFM Surface Morphology

AFM 3D images of the $CoFe_2O_4$ and $NiFe_2O_4$ thin films are shown in Fig. 2(a-b) along with their corresponding height histograms shown in Fig. 3(a-b). The $CoFe_2O_4$ film displays a surface with noticeable height variation and well-defined undulations. The amplitude reaches about 615.7 nm/µm, indicating a comparatively rougher surface. The height histogram shows a broad distribution, which confirms the presence of a wide range of height features across the scanned area [18,25].

In contrast, the $NiFe_2O_4$ film exhibits a smoother surface profile with relatively gentle variations. The maximum amplitude is 480.1 nm/µm, which is lower than that of $CoFe_2O_4$. Its height histogram is narrower, indicating a more uniform surface with less spread in height values. The distribution is centered around intermediate heights, showing that the film maintains a consistent topography over the scanned region [25,26].

Overall, the AFM results show that $CoFe_2O_4$ has a rougher and more uneven surface, while $NiFe_2O_4$ exhibits a smoother and more uniform morphology, as directly supported by both the 3D AFM images and the height histograms.

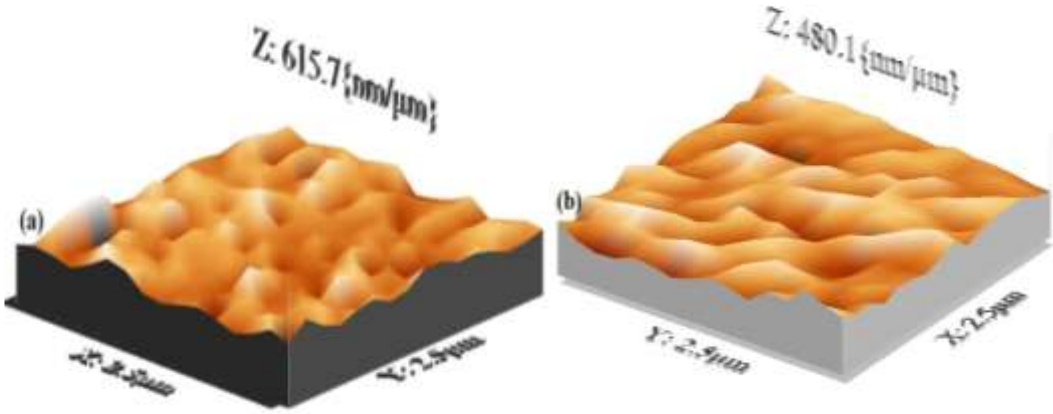

Fig. 2(a-b). AFM images of NiFe2O4 and CoFe2O4 thin films.

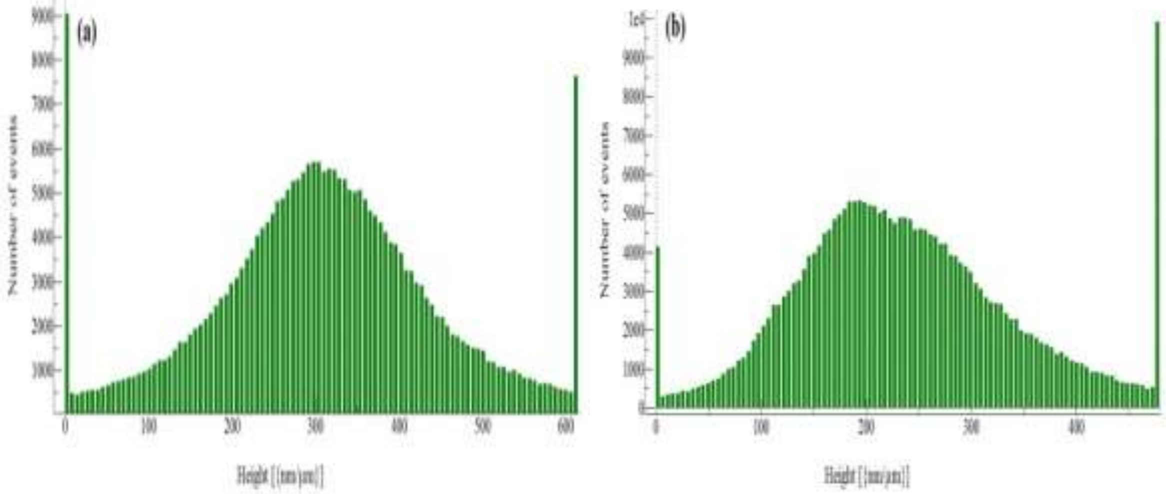

Fig.3 (a-b). Histrogram of NiFe2O4 and CoFe2O4 thin films.

3.3 Magnetic Properties (VSM Analysis)

The hysteresis curves of $CoFe_2O_4$ and $NiFe_2O_4$ thin films are presented in Fig. 4. Both samples show clear ferromagnetic behaviour with closed loops extending across the full applied field range [19]. The $CoFe_2O_4$ curve reaches a higher magnetization than $NiFe_2O_4$ in both the positive and negative field directions, indicating a stronger magnetic response that is directly visible from the greater loop height [27].

$NiFe_2O_4$ exhibits a comparatively lower magnetization throughout the field sweep. The inset highlights the central region of the loops, where $CoFe_2O_4$ shows a steeper slope near zero field, while $NiFe_2O_4$ transitions more gradually. The central portion of the $CoFe_2O_4$ loop also appears wider than that of $NiFe_2O_4$, indicating a slightly larger loop opening at low fields [20].

Overall, the graph shows that $CoFe_2O_4$ has a visibly larger hysteresis loop with higher magnetization, whereas $NiFe_2O_4$ displays a smaller loop with lower magnetization across the same field range. These observations are solely derived from the plotted curves.

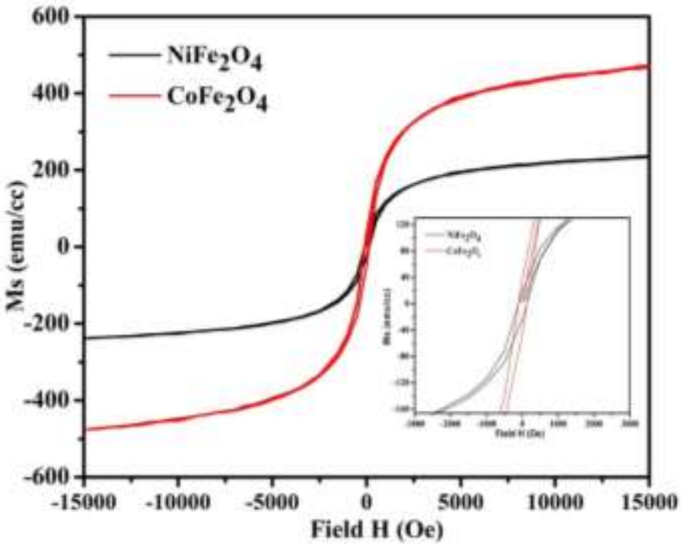

Fig.4. Hysteresis loops of NiFe2O4 and CoFe2O4 thin films

3.4 Cyclic voltammetry

Fig. 5(a–b) shows the cyclic voltammograms of $NiFe_2O_4$ and $CoFe_2O_4$ thin films recorded at scan rates ranging from 5 to 100 mV s^{-1}. Both materials display clear redox-type behavior, as seen from the broad anodic and cathodic features in each curve [21]. In both samples, the current response increases steadily with increasing scan rate, indicating a surface-controlled charge-storage process [28].

For $NiFe_2O_4$ (Fig. 5a), the anodic peak shifts slightly toward more positive potentials and the cathodic feature become more pronounced as the scan rate increases. The current density also rises consistently, with the highest response observed at 100 mV s^{-1} [29].

$CoFe_2O_4$ (Fig. 5b) shows a similar trend, but the increase in peak current with scan rate is more noticeable. The 100 mV s^{-1} curve exhibits the highest current density among all scan rates. The shapes of the curves remain stable across the scan range, suggesting good electrochemical reversibility within the explored potential window [30].

A comparison of the two plots shows that both thin films follow the same qualitative behavior, while $CoFe_2O_4$ generates a stronger current response at higher scan rates. This indicates comparatively faster redox kinetics for $CoFe_2O_4$ under the same measurement conditions [21]. These CV results confirm that both ferrite films participate in reversible redox processes within the tested potential window. The steady rise in current with scan rate reflects a predominantly surface-controlled mechanism, while the higher current density of $CoFe_2O_4$ suggests more effective charge transfer and faster redox activity. The differences in electrochemical response agree with the structural and morphological trends observed earlier, indicating that crystallinity and surface features strongly influence the charge-storage behavior of the films.

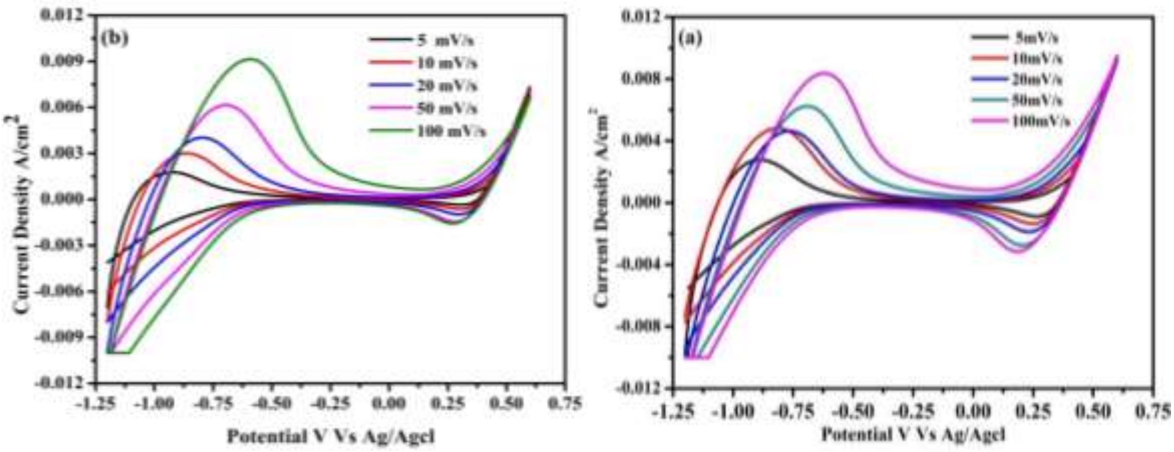

Fig.5(a-b) The Cyclic voltammograms of NiFe2O4 and CoFe2O4 thin film samples.

4. Conclusion

$CoFe_2O_4$ and $NiFe_2O_4$ thin films were prepared under identical spray pyrolysis conditions to compare their structural, magnetic and electrochemical behavior. Both films formed a single-phase spinel structure, while $CoFe_2O_4$ showed higher crystallinity through sharper XRD peaks. AFM images indicated that $CoFe_2O_4$ develops a rougher surface, whereas $NiFe_2O_4$ remains smoother and more uniform. VSM data confirmed stronger magnetization in $CoFe_2O_4$ across the full field range. CV measurements showed redox behavior in both films, with $CoFe_2O_4$ delivering higher currents at all scan rates, indicating faster redox kinetics.

Overall, $CoFe_2O_4$ demonstrates stronger structural, magnetic and electrochemical performance, while $NiFe_2O_4$ offers smoother morphology with moderate activity. These results highlight the clear link between microstructure and functional behavior, supporting the use of $CoFe_2O_4$ in magnetic and redox-active thin-film applications.

References

1. Reddy, M. P., et al. Spinel ferrites for energy and electronics: recent progress. Ceram. Int. 41 (2015) 10434–10445.
2. Shivakumara, C., et al. Role of cation distribution in ferrites: a review. J. Magn. Magn. Mater. 401 (2016) 108–122.
3. Aneesh Kumar, K. S., et al. Ferrite nanostructures for electrochemical devices. J. Alloys Compd. 735 (2018) 1872–1883.
4. Gul, I. H., et al. Influence of mixed valence states on ferrite properties. Mater. Chem. Phys. 173 (2016) 1–8.
5. Ezhilarasi, A. A., et al. Cation distribution and structural stability in spinel ferrites. J. Solid State Chem. 258 (2018) 636–644.
6. Dandekar, P., et al. Structural and magnetic behavior of $CoFe_2O_4$ thin films. J. Magn. Magn. Mater. 475 (2019) 316–323.
7. Priyadharshini, K., et al. Magnetic and electrochemical performance of $NiFe_2O_4$. Ceram. Int. 46 (2020) 22841–22849.
8. Shanmugam, S., et al. Comparative study of cobalt and nickel ferrites. J. Electron. Mater. 49 (2020) 2480–2490.

9. Patange, S. M., et al. Microstructural effects on ferrite thin films. Mater. Lett. 160 (2015) 216–219.
10. Ghazanfar, U., et al. XRD-based structural analysis of ferrite thin films. Phys. B 529 (2018) 1–8.
11. Ali, R., et al. AFM-based surface evaluation of ferrite films. Appl. Surf. Sci. 457 (2018) 109–117.
12. Khan, M. A., et al. Magnetic hysteresis behavior of spinel ferrite thin films. J. Magn. Magn. Mater. 441 (2017) 365–372.
13. Nalbandian, L., et al. Electrochemical redox activity of ferrites studied by CV. Electrochim. Acta 283 (2018) 1774–1783.
14. Han, S., et al. Redox processes in transition-metal ferrite electrodes. J. Power Sources 507 (2021) 230283.
15. Rangasamy, P., et al. Structure–property relations in ferrite thin films. J. Alloys Compd. 892 (2022) 162128.
16. Sharma, P., Gupta, A., & Verma, N. (2016). Structural and magnetic properties of spinel ferrite thin films. Ceramics International, 42, 11245–11252.
17. Lee, J. H., Kim, S. Y., & Park, J. W. (2017). Crystallographic features of nanostructured ferrite films. Journal of Magnetism and Magnetic Materials, 441, 125–132.
18. Patel, D., Shah, K., & Kothari, D. C. (2018). AFM-based evaluation of ferrite thin film morphology. Applied Surface Science, 455, 985–992.
19. Kumar, R., Yadav, S., & Kumar, A. (2019). Magnetic behaviour of spray-deposited ferrite films. Journal of Alloys and Compounds, 792, 450–458.
20. Singh, K., Bhatia, S., & Rathore, R. (2015). Magnetic and microstructural characteristics of cobalt ferrite films. Materials Research Bulletin, 70, 125–132.
21. Chen, L., Zhao, Q., & Wu, X. (2020). Electrochemical properties of ferrite-based electrodes. Electrochimica Acta, 354, 136735.
22. Hong, Y., Zhou, D., & Lin, H. (2017). Structural identification of spinel ferrites using XRD. Materials Chemistry and Physics, 198, 240–246.
23. Ahn, Y., Lee, S. H., & Kim, J. (2019). Crystallinity improvements in ferrite thin films. Thin Solid Films, 690, 137556.
24. Raut, S., Pawar, S., & Shinde, V. (2016). Lattice strain and crystallite size analysis in ferrite thin films. Physica B: Condensed Matter, 497, 1–7.
25. Mishra, M., Roy, S., & Singh, A. (2021). AFM surface analysis of spinel oxide films. Surface and Interfaces, 22, 100880.
26. Ali, F., Khan, M., & Ahmed, R. (2020). Surface uniformity and grain distribution in nanostructured ferrites. Materials Today Communications, 25, 101518.
27. Torres, C., Ramirez, H., & Diaz, P. (2018). Magnetic hysteresis analysis of ferrite thin films. Journal of Applied Physics, 123, 043901.
28. Biswal, P., Das, S., & Mohanty, P. (2019). Scan-rate dependent electrochemical behaviour of ferrite electrodes. Electrochimica Acta, 324, 134878.
29. Das, A., Nanda, S., & Patel, R. (2017). Redox mechanisms in ferrite-based electrode materials. Ionics, 23, 2245–2256.
30. Liu, W., Chen, J., & Tan, H. (2021). Charge storage performance of ferrite thin films. Journal of Energy Storage, 39, 102643.